

Study on flow field structure and dust suspension law in tunnel construction drilling process

Xiang Fan, Zhijun Huang^{a*}

School of Civil Engineering Lanzhou Jiaotong University, Gansu Lanzhou 730070, China

Abstract. In order to clarify the dust production law of railway tunnel drilling and blasting construction, the flow field structure characteristics and the distribution and migration law of drilling dust production in the tunnel under the condition of press-in ventilation were studied by indoor model test and CFD numerical simulation method. The results show that: 1) The dust concentration on the M axis and R axis gradually decreases with the increase of distance from the face of the face. The dust concentration on the L axis showed a small-large-small trend from the palm surface to the outlet of the hair dryer, and the maximum dust concentration appeared at 1m away from the face of the face. 2) Under the condition of press-in ventilation, the flow field structure can be divided into three parts: jet area, vortex area and reflux area, and the proportion of reflux gradually increases from 54% to 100% after three stages. 3) Large particles of dust mainly settle in the area of 1m from the end of the working face on the return air side, and the particle size of the dust settled on the tunnel floor gradually decreases with the increase of the distance from the face face; Most dust particles can settle or discharge the tunnel within 30s, and the vortex area has an adverse effect on the tunnel dust exhaust and dust reduction.

1 Introduction

As an important and economical construction method, the borehole blasting method is widely used in the construction of rock tunnels, but the construction dust generated seriously threatens the health of workers.

In view of the problem of tunnel production dust control and protection, many scholars have conducted a lot of research on the dust migration law with the help of numerical simulation technology. Gabriel Arpa et al. [1] studied the turbulent diffusion phenomenon of mine ventilation channels by using the movement of discrete particles in the injected ventilation airstream in a numerical model, and determined the effective diffusion coefficient of the diffuse particle belt. Stovern et al. [2] studied the dust migration and diffusion law of mine tailings through field measurements and computational fluid dynamics modeling, and concluded that boundary conditions and wind speed are the main factors affecting dust movement. Zou Zongliang et al. [3] explored the diffusion law of harmful gases and dust in tunnel blasting operations by numerical means, and took relevant control measures Cao Zhengmao [4] further explored the dust migration law and dust mass concentration distribution characteristics during tunnel construction at different altitudes. Nie Xingxin et al. [5] used FLUENT to simulate the positions of different air supply ducts and dust removal ducts and pumping pressure ratio parameters of the TBM construction tunnel at plateau under the long pressure and short pumping mode, analyzed the migration characteristics of

dust in the tunnel, and optimized the layout of the ventilation system. Scholars [6–8] also studied the dust migration distribution of tunnel dust under different ventilation conditions through numerical simulation, and proposed corresponding optimized dust reduction measures on this basis. Some scholars have combined similar theories with practical gas-solid two-phase flow engineering problems to study the migration law of dust movement: Ge Lianmeng et al. [9] studied the dust distribution and diffusion characteristics of high chute discharge.

CFD numerical simulation and model test have become a powerful tool to analyze the characteristics of two-phase flow field and dust movement and migration, this paper studies the change characteristics of wind speed and dust concentration in the center height of the tunnel duct through model tests, and further analyzes the overall structure of the model flow field and dust distribution by combining numerical methods, in order to provide theoretical support for improving the working environment in the tunnel and optimizing the tunnel ventilation and dust reduction system.

2 Similar trial designs

2.1. Gas-solid two-phase flow equation

The equation is used to describe the physical phenomenon of gas-solid two-phase flow in the construction of tunnel drilling and blasting method,

* Corresponding author: 543768854@qq.com

which should include two parts: wind flow movement and particle movement. Assuming that the space inside the tunnel is an isothermal field and the gas inside the tunnel is regarded as an incompressible viscous gas, the governing equation for the continuous phase is:

$$\rho_g \left(\frac{\partial U_g}{\partial t} + U_g \cdot \nabla U_g \right) = m - \nabla P + \mu_g \nabla^2 U_g \quad (1)$$

where ρ_g is the density of the gas, kg/m^3 ; U_g is the gas velocity, m/s ; ∇U_g is the velocity gradient; m is the unit mass force vector of the gas, $m = \rho_g g$, N/m^2 ; P is the pressure vector of the gas, Pa (∇P is the pressure gradient); $\mu_g \nabla^2 U_g$ are force vectors other than mass force and gas pressure; μ_g is the viscosity coefficient of the gas, $\text{N}\cdot\text{s/m}^2$; g is the acceleration due to gravity, m/s^2 .

The migration and diffusion of tunnel dust in the tunnel is affected by three different types of forces: one is the interaction force between particles; The second type is the force determined by the properties of the particle itself, which has nothing to do with the flow field motion; The third category is the force related to the motion of the flow field. For the sake of analysis and calculation, the dust in the tunnel is treated as spherical particles. Due to the migration characteristics of dust particles, they are less affected by the first type of force; In practice, the density of the particle phase is much greater than that of the continuous phase, so the influence of additional mass force and Basset force on the dust can be ignored. Saffman's lift is positively correlated with the velocity gradient of the flow field, and the velocity gradient is small in the main stream of the flow field, which only becomes obvious in the velocity boundary layer, but the research object is the whole roadway, and the laminar bottom layer with a large velocity gradient accounts for only a very small part, so the influence of Saffman's lift is also ignored [10]. Similarly, the proportion of dust that rotates throughout the tunnel is smaller, so the action of the Magnus force is ignored. By ignoring the higher-order small forces of the dust and taking into account the magnitude of the various forces on the particles (as shown in Table 1), according to Newton's second law, the discrete phase equation is:

$$\frac{1}{6} \pi d^3 \rho_p \frac{dU_p}{dt} = \frac{1}{8} C_D \pi d^2 \rho_g V_r |V_r| \quad (2)$$

where ρ_p is the particle density, kg/m^3 , and d is the particle diameter, m ; C_D is the drag coefficient, and V_r is the relative velocity of the gas-solid phase, m/s .

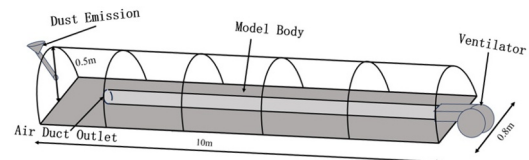
2.2 Number of similar criteria vs. simplification

From equations (1) and (2), it can be seen that there are 10 quantities with dimensions, namely ρ_g , ρ_p , U_g , U_p , P , μ_g , d , g , l , t , and the basic physical dimensions only T (time), M (mass), L (length), and 10 independent similarity criteria can be deduced according to the similarity of dimensional analysis and single-value conditions: Stokes criterion, Euler criterion, Reynolds

criterion, velocity criterion, density criterion, uniformity criterion, Froude criterion, Reynolds particle criterion, roughness criterion, and geometric criterion. In practice, it is not possible for the tunnel similarity model and the prototype to satisfy all the similarity criteria at the same time, so the similarity criterion must be simplified. In this paper, according to the actual situation of gas-solid two-phase flow in tunnels, the similarity criteria that need to be satisfied in theoretical derivation are simplified into Stokes criterion, Reynolds particle criterion, roughness criterion and geometric criterion. If the test platform is designed according to the similarity ratio $C_{I_M} : I_R = 10$, the test wind speed should be 10 times of the actual wind speed, and the $R_c = l \rho_g v_g / \mu_g$ is calculated according to the formula $R_c > 2300$, and the fluid is in a turbulent state, so the test wind flow speed only needs to meet the similarity of the dynamics.

2.3 Platform construction and measurement point layout

According to the above conditions, a similar test platform can simulate the ambient wind speed in the tunnel, which is mainly composed of three parts: the main structure of the model, the ventilation system and the dust generation system. A dust generating device is installed in the center of the tunnel face of the model to simulate the dust generation of the borehole, and a ventilation system is established to provide power for the movement of dust in the model. The model is a horseshoe-shaped tunnel with a cross-section width of 0.8m, a height of 0.5 m, and a total length of 10 m, with a diameter of 0.15 m for the hair duct, placed on the left side of the model tunnel, and the air outlet of the air duct is 2m away from the face of the tunnel. A similar test platform is shown in Figure 1.



(a) Model design drawing



(b) Model physical image

Figure 1 Similar test model

Inside the model, 3 axes were set from left to right on the palm surface, denoted as L axis, M axis and R axis, respectively, and sampling points were set at a certain distance between each axis. During the test, the wind speed at the outlet of the duct was controlled to be 5m/s and the dust generation mode was continuous dust generation. The thermal anemometer and CCHG1000 direct-reading dust concentration measuring instrument were respectively used to measure the wind speed and

dust mass concentration at the sampling point. The average value of the wind speed and dust mass concentration at each measuring point was measured three times and the sampling time of the dust meter was set to 2 minutes. The sampling point arrangement of the test is shown in Figure 2.

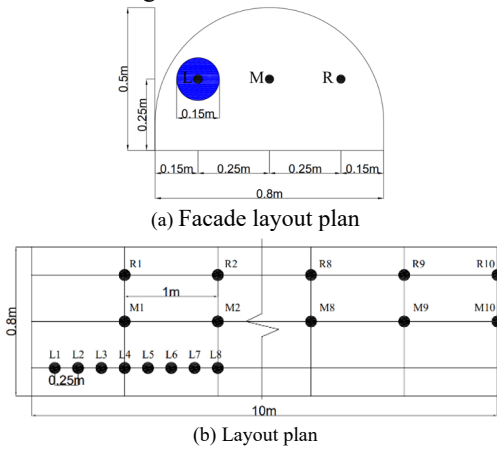


Figure 2 Measurement point layout

2.4 Test results and analysis

Based on the above conditions, the influence of jet on tunnel flow field distribution and dust concentration distribution is studied, and the test results are shown in Figure 3.

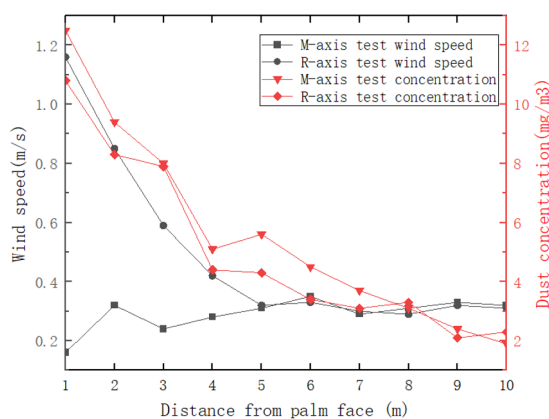
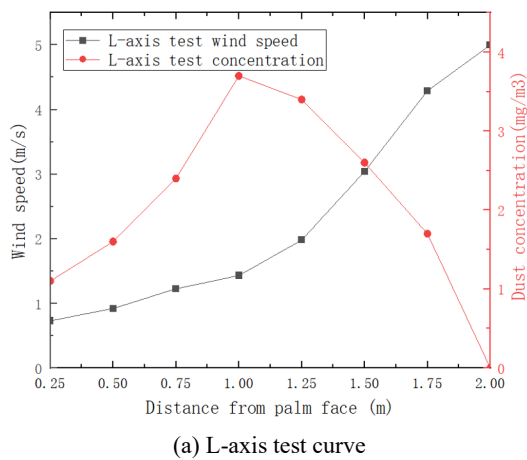


Figure 3: Test data graph

The analysis combined with Figure 3 shows that the wind speed of the flow field in the tunnel in the area of the palm face and duct is $L > R > M$, and the overall performance is that the jet wind speed is greater than the wind speed on the return air side than the wind speed in the middle of the tunnel. In the middle area of the tunnel, due to the influence of the air duct jet, eddy currents are generated during the energy conversion process, which leads to fluctuations in the wind speed in this area. The wind speed from the outlet of the wind duct to the face of the palm gradually decreases, while the wind speed away from the side of the wind duct gradually decreases with the increase of the distance from the face of the palm until 5m away from the face of the palm, the wind speed basically remains unchanged.

At the same time, the dust concentration in the area between the air duct and the face of the palm is different, and the dust concentration on the side of the air duct is low due to the fresh air flow. In the middle of the model, due to the existence of eddy current, dust particles are difficult to settle or eliminate in time, so this area has the highest concentration; Because some dust migrated to the return air side with the jet movement, the dust concentration at the return air side was higher. On axis L, the dust concentration presents a small-large-small trend from the face of the palm to the outlet of the air duct, and the maximum dust concentration appears at 1m away from the face of the palm: fresh jet enters through the outlet of the air duct, and the dust mass concentration near the outlet is relatively low. With the increase of jet distance, the suction effect of jet on the surrounding dust-bearing air will increase the dust concentration to a certain extent. When the jet moves to the vicinity of the palm surface, the diffusion of the jet and the movement of dust in the area near the palm surface mainly to the return air side under the action of air flow cause the dust concentration to gradually decrease. On the M-axis and R-axis, the dust concentration gradually decreases with the increase of the distance from the palm surface, and basically tends to be stable after reaching a certain distance. At this time, the dust particles are difficult to settle, which is mainly eliminated through the carrying effect of wind flow. The reduction of dust concentration in the model mainly depends on the carrying effect of gravity and wind flow. Due to the eddy current in the middle of the model, the dust in this region is difficult to settle in time, so the large particles of dust mainly settle in the return air side. Comparing the curves in the figure, it is not difficult to find that the distribution of wind speed in the model has a significant influence on the distribution of dust concentration: when the wind speed changes greatly, the dust concentration changes significantly, and when the wind speed tends to be stable, the dust concentration also tends to be stable. The concentration peaks appear in the local region of the model, which is because there are many vortex structures in the micro-upstream field and the vortex regions of different sizes are formed in the macro-level.

3 Based on computational fluid dynamics numerical simulation

Due to the limitations of the indoor model test conditions, the test only obtained the test values of some key points, which could not reflect the overall picture of wind speed and dust concentration distribution in the tunnel. However, by means of numerical simulation, the flow field and dust concentration distribution in the tunnel could be obtained in detail, and the simulation results could be mutually corroborated with the test results.

3.1. Establish geometric model and parameter setting

A physical model of the same size as a similar test platform is built in SPACECLIAM, and the geometric model is unstructured meshed using ICEM, as shown in Figure 4. In the three-dimensional model, the left direction of the vertical axis is the positive direction of the X axis, the tunnel axis points to the tunnel exit direction is the positive direction of the Y axis, and the vertical axis points to the arch top direction is the positive direction of the Z axis. The model boundary consists of four parts: entrance, exit, particle injection source and wall surface.

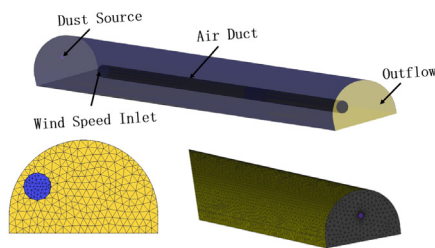


Figure 4 Physical model and mesh

Since the exit of a similar model is an atmospheric environment, the exit type can be set to outflow. The outlet of the duct is the source of air flow, and the wind speed at the outlet is set to 5 m/s. The Rosin-Ramler (R-R) distribution of dust particles was selected, and the standard $k-\epsilon$ equation and SIMPLEC algorithm were used to simulate the particle size distribution. The single-phase air flow field was first solved, and the discrete phase dust source was created after the single-phase air flow field convergence. The DPM model was used for coupling calculation and solution with the continuous phase. Please refer to Tables 1 and 2 for other related settings.

Table 1 Boundary Settings

Solver	Pressure-Based
Turbulence model	Standard k-
Inlet Boundary Type	velocity-inlet
Outlet Boundary Type	Outflow
Wall Shear Condition	No Slip
Pressure-Velocity Coupling	SIMPLEC

Table 2 Dust Source Settings

Interaction with Continuous Phase	On
Length Scale	0.1
Injection type	Surface
Discrete Random Walk Model	On
DPM Boundary Type	Reflect/trap
Diameter Distribution	R-R

3.2 Distribution of flow field in tunnel

In the process of tunnel drilling, a large amount of dust generated by the mechanical friction between the drill bit and the rock on the face of the palm is rapidly diffused and diffused in the space near the face of the palm under the action of wind flow. Therefore, clarifying the flow law of air flow field in the tunnel is the basis for studying the movement and migration law of dust in the tunnel. The wind speed distribution cloud diagram and wind speed vector diagram of some sections are extracted from the simulation results, as shown in Figure 5:

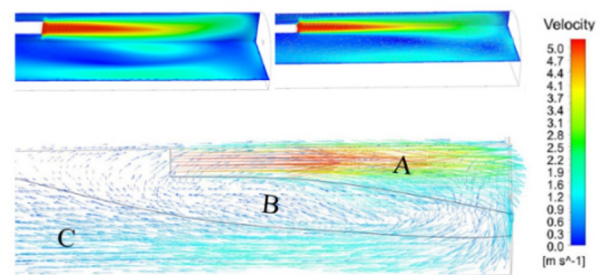


Figure 5 Flow field structure

Figure 5 shows that in the process of fresh air flow from the outside world shooting towards the palm surface through the duct outlet under the action of the fan, the fresh air flow mixes with the original gas in the tunnel, resulting in the conversion of energy and momentum. As a result, the wind speed of the ejector fluid gradually decreases with the increase of the distance along the road, and the air flow section keeps expanding. At the same time, due to the constraint effect of the palm surface and the tunnel wall, the direction of air flow gradually deviates to the other side of the tunnel, and the final direction of air flow returns in front of the palm to form a reflux, which runs towards the tunnel exit direction. At the same time, in the local area between the jet and the reflux, there are a large number of vortices formed by the mutual interference of turbulence in different directions, which appear as vortex region in the macroscopic view. Therefore, the air flow structure in the tunnel can be roughly divided into three parts: the left arch at the exit of the air duct in the tunnel is the jet zone, the other side is the reflux zone, and there is A vortex zone between the jet zone and the reflux zone, corresponding to the three places A, B and C in the figure respectively.

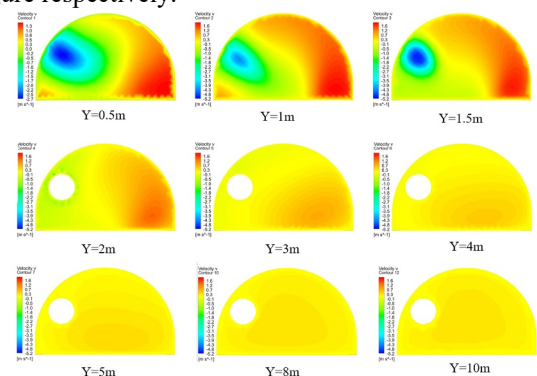


Figure 6 Velocity distribution cloud in Y direction

The concentration of tunnel dust is reduced in two ways. First, the rapid sedimentation of large-diameter particles is mainly under the action of gravity, which mainly occurs near the palm surface. Second, through the carrying effect of reflux air flow in the tunnel space from the high concentration area to the low concentration area, mainly small particle size, generally occurs in the tunnel space at a certain distance from the palm surface. Therefore, the proportion of the return area in the tunnel flow field structure has a significant impact on the ventilation dust removal effect, expressed as the percentage of the return area in the tunnel cross-section, which is specifically expressed as the percentage of the area with velocity greater than zero along the Y axis in the entire section of the ZX cross-section. FIG. 6 shows the velocity distribution cloud map in the Y direction on the ZX section at different distances from the palm plane, where the positive velocity represents the reflux and the negative velocity represents the jet. The backflow area increased gradually from the right side of the tunnel to the left side of the tunnel. The negative velocity area between the wind duct outlet and the palm surface is constantly increasing, because the impact jet has an enrolling effect on the surrounding gas, and the surrounding air is forced to move towards the palm surface along the way.

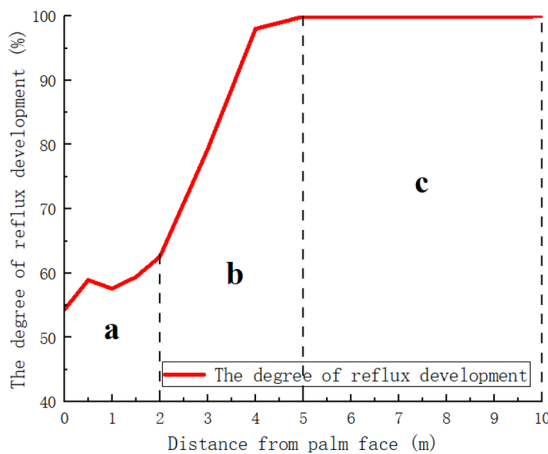


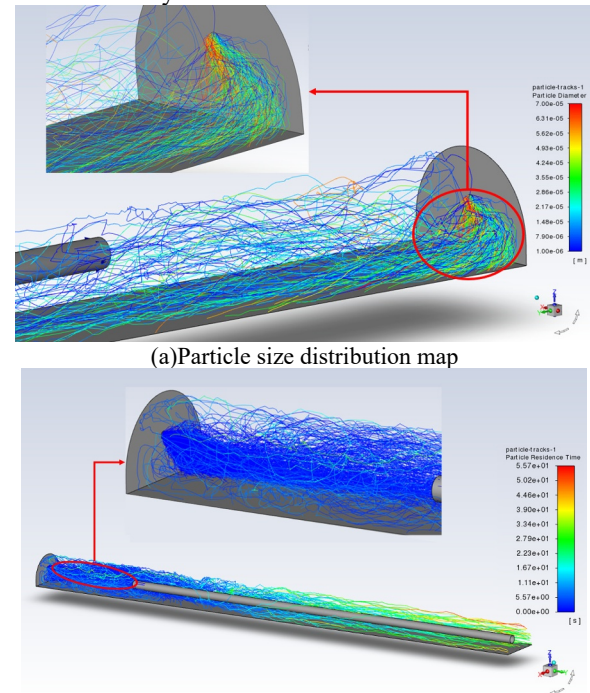
Figure 7 Reflux development trend

Figure 7 shows the development curve of the reflux area, which can be divided into three stages: Stage a corresponds to the area between the outlet of the duct and the face of the palm, where there is a joint action of jet zone, vortex zone and reflux zone, resulting in slow reflux development; Stage b corresponds to the area 2-5m away from the palm surface. There is no direct influence of jet in this area, only a small part of eddy current is affected locally, and reflux develops rapidly. Stage c reflux basically extends to the entire tunnel space, corresponding to the area 5m from the palm surface to the model exit.

3.3 The influence of flow field on the law of dust diffusion and migration

Based on the above analysis of the structure of the pressurized ventilation field, numerical simulation of the dust field under the pressurized ventilation condition of

the model test tunnel was carried out, and the particle trace diagram of the flow field was extracted from the simulation results (as shown in FIG. 8) to conduct simulation analysis of the dust field.

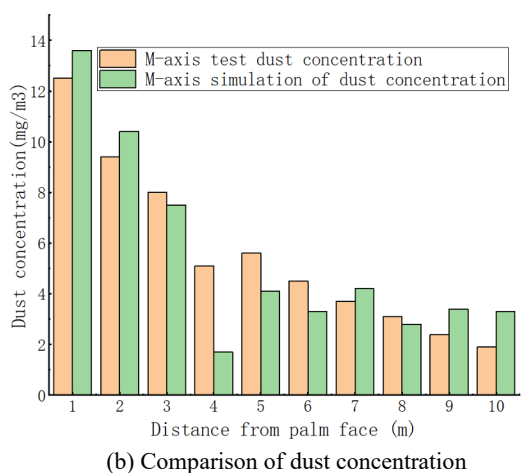
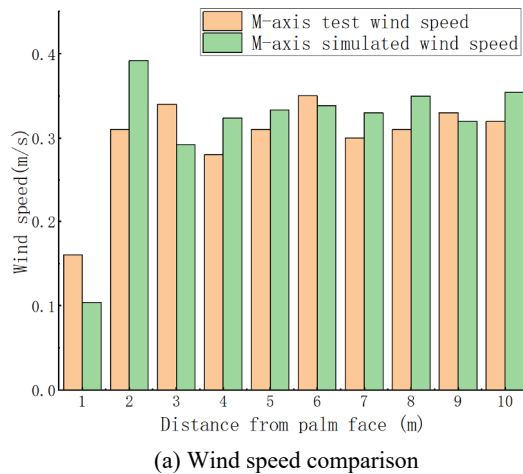


(a) Particle size distribution map
 (b) Particle residence time graph
Figure 8 Particle size diagram of flow field

Figure 8 shows that the initial velocity of the dust released from the dust source is low, and the dust released from the palm surface into the tunnel space is affected by air flow field and dust gravity, etc. Large particles of dust are greatly affected by gravity and rapidly settle on the return air side near the palm surface. The resistance coefficient of small particles is small, the lifting force and gravity are easy to reach a balance state, and it is not easy to settle when suspended in the tunnel, mainly relying on the wind flow to move from the palm to the exit direction. Most dust particles can settle or discharge from the tunnel within 30s, but some dust stays in the area between the wind duct and the face of the palm for a long time. This is because the air duct jet continuously enrolls dust from the vortex zone, and part of the dust circulates in the vortex zone with the air flow, which increases the particle migration time and has an adverse effect on the dust removal and fall of the tunnel. The vertical distribution of dust in front of the palm showed an obvious stratification phenomenon, and the dust concentration in the same section from the arch top to the bottom floor showed a law from small to large and then small, which was due to the difference in the molecular weight of dust, the gravity of large particles was greater than the lift force of the flow field, and the settlement trend was significant. In the horizontal direction, dust moves to the return air side under the action of flow field and air flow, and is limited by the wall surface. When the air flow is near the wall, the power provided by the dust particles will become weaker, resulting in the overall trend of the dust mass concentration in the horizontal direction from small to large and then small from left to right.

4 Contrast verification

Through the analysis of the results of model test and numerical simulation, it is not difficult to find that the two have good consistency in wind speed and dust concentration distribution. Take M-axis as an example, extract test data and simulation values of measuring points on M-axis and draw a bar chart, as shown in Figure 7.



(a) Wind speed comparison
 (b) Comparison of dust concentration
Figure 9 M-axis verification comparison chart

Comparing the two figures, it can be seen that the distribution rules of model wind speed and dust concentration obtained by numerical simulation are basically the same as the model test results, but there are some deviations in the local values of the two methods, which is caused by the test conditions and errors. On the whole, the experimental data are in good agreement with the simulated data, and the deviation between them is within a reasonable range, so the research results are credible.

5 Conclusions

1) The dust concentration on the L axis presents a small-large-small trend from the palm surface to the outlet of the ventilator, and the maximum dust concentration appears at 1m away from the palm surface; On the M-axis and R-axis, the dust concentration gradually decreases with the increase of the distance from the palm

surface, and basically tends to be stable after reaching a certain distance. At this time, the dust particles are difficult to settle, which is mainly eliminated through the carrying effect of wind flow.

2) Under the condition of pressurized ventilation, the flow field structure can be divided into three parts: jet zone, vortex zone and reflux zone, in which the jet zone and vortex zone are mainly distributed in the area between the wind duct and the palm surface, and the reflux zone is widely distributed throughout the tunnel. Within 0-2m distance from the face of the palm, the proportion of reflux area slowly developed from 54% to about 63%. The proportion of reflux area in 2-5m distance from the palm surface developed rapidly from 63% to more than 98%. The reflux area 5-10m away from the palm surface basically developed into this tunnel space, and the proportion of the reflux area was close to 100%.

3) Large particle dust mainly settles within 1m from the end of the working face on the return air side, and the particle size of dust settling on the tunnel floor gradually decreases with the increase of the distance from the palm face; Most of the dust particles can settle or discharge from the tunnel within 30s, and some dust stays in the vortex zone for a long time. The vortex zone has an adverse effect on the tunnel dust discharge and fall.

References

1. Gabriel Arpa, Arif Widiatmojo, Nuhindro Priagung Widodo, et al. Tracer gas measurement and simulation of turbulent diffusion in mine ventilation airways[J]. *Journal of Coal Science and Engineering (China)*, 2008, 14(4): 523–529.
2. Stovern M, Felix O, Csavina J, et al. Simulation of windblown dust transport from a mine tailings impoundment using a computational fluid dynamics model[J]. *Aeolian Research*, 2014, 14: 75–83.
3. ZOU Zongliang, HU Xuebing, YUAN Ye, et al. Study on the influence law of blasting operation on CO and dust diffusion in high altitude tunnel [J]. *China Highway* 2022, (11), 150-152
4. CAO Zhengmao, LIU Xiao, NIU Baichuan. Migration Characteristics of Dust during Construction Stage in Highway Tunnels at High Altitude Areas [J]. *Chinese Journal of Underground Space and Engineering*, 2019, 15(3): 927–935.
5. NIE Xingxin, LI Kaipeng, HONG Yong, et al. Study on dust transport characteristics and ventilation system arrangement for high altitude tunnel construction [J]. *Journal of Safety and Environment*, 1-9[2023-12-20].
6. JIANG Zhongan, WANG Yapeng, MEN Liguu. Ventilation control of tunnel drilling dust based on numerical simulation [J]. *Journal of Central South University*, 2021, 28(5): 1342–1356.
7. LIU Yazhou, XIAO Junfeng, LU Ping, et al. Simulation Study of Dust Removal in Far-Pressing-Near-Absorption Ventilation of Nanshan Highway

- Tunnel [J]. Journal of Tongling University , 2019, 18(6): 98–101.
8. ZHAO Shulei, WANG Haiyang, ZHAO Ningyu, et al. Migration Law of Pollutants under Dead-End Limit Ventilation Distance of Milashan Tunnel [J]. Tunnel Construction, 2021, 41(S2): 367–374.
 9. GE Lianmeng, WANG Linhong, CHEN Yihua, et al. Experimental Study on Dust Diffusion Characteristics of High Pass [J]. Modern Mining, 2021, 37(2): 167–172.
 10. QI Yipei. Research on Airflow Energy Dissipation Mechanism and Dust Transport Model of Roadway [D]. Beijing : China University of Mining and Technology, 2021.